Supporting Information

Superconducting $Li_{11}Sb_2$ electride at ambient pressure

Yaping Zhao†, Jiayu Gao†, Xiaohua Zhang*, Shicong Ding, Yong Liu, and Guochun Yang*
State Key Laboratory of Metastable Materials Science & Technology and Key Laboratory for Microstructural Material Physics of Hebei Province, School of Science, Yanshan University, Qinhuangdao 066004, China
†Y.Z. and J.G. contributed equally.

Computational Details

The structural prediction method is based on a global minimization of free energy surfaces merging *ab initio* total-energy calculations with the CALYPSO (Crystal structure AnaLYsis by Particle Swarm Optimization) method.[1, 2] We carry out a structural search on Li_xSb_y (x = 3-10, and y = 1; x = 5, 7, 9, 11, 13, 15, and y = 2) at 0 K and select pressures of 50, 100, 200, and 300 GPa. In the first step, random structures with certain symmetry are built with atomic coordinates generated by crystallographic symmetry operations. Local optimizations using the VASP code[3] are done with the conjugate gradient method and stopped when enthalpy changes became smaller than 1×10^{-5} eV per cell. After processing first generation structures, 60% of them with lower enthalpies are selected to construct the next generation with PSO (Particle Swarm Optimization). 40% of the structures in the new generation are randomly generated. A structure fingerprinting technique of bond characterization matrix is applied to the generated structures, so that identical structures are strictly forbidden. These procedures significantly enhance the diversity of the structures, which is crucial for the structural global search efficiency. In most cases, structural searching simulations for each calculation were stopped after generating 1000 ~ 1500 structures (e.g., about 20 ~ 30 generations).

In order to further analyze the structures with higher accuracy, we select a number of structures with lower enthalpies and perform a structural optimization using density functional theory (DFT) with the generalized gradient approximation (GGA) as implemented in the VASP code.[4-6] In all the calculations the cut-off energy for the expansion of wavefunctions in plane waves is set to 800 eV, and the Monkhorst-Pack k-meshes with a grid spacing of $2\pi \times 0.03$ Å^{-1} are selected to meet the energy convergence.[7] The electron-ion interaction is described by the projector augmented-wave method (PAW)[8] with $1s^2 2s^1$ and $5s^2 5p^3$ valence electrons for Li and Sb, respectively. The dynamic stability

was confirmed by phonon dispersion curves calculated with the PHONOPY code.[9]

To further test the reliability of the adopted pseudopotentials for Li and Sb, the validity of the projector augmented wave pseudopotentials from the VASP library are checked by comparing the calculated Birch-Murnaghan equation of state with those obtained using the full-potential linearized augmented plane-wave method (LAPW, as implemented in WIEN2k),[10] which uses local orbitals. The Birch-Murnaghan equation of states derived from PAW and LAPW methods are almost identical. Thus, our adopted PAW potentials are reliable in the range of 0-300 GPa.

The *ab*-initio molecular dynamics (AIMD) simulations last 10 ps with a time step of 1 fs and are based on an NVT ensemble with Nosé-Hoover temperature control[11]

The electron-phonon coupling (EPC) calculations are performed within PWscf (Plane-Wave Self-Consistent Field) package in QUANTUM ESPRESSO.[12] For high pressure phase, we employ ultrasoft pseudopotentials of li_pbe_v1.4.uspp.F.UPF and sb_pbe_v1.4.uspp.F.UPF. The *C*2/*m* $Li_{11}Sb_2$-II structure at 0 GPa is calculated by using Norm-conserving pseudopotentials of Li.pz-mt_fhi.UPF and Sb.pz-mt_fhi.UPF. The T_c is estimated from the McMillan-Allen-Dynes formula:[13, 14]

$$T_c = \frac{\omega_{log}}{1.2} exp\left[-\frac{1.04(1 + \lambda)}{\lambda - \mu^*(1 + 0.62\lambda)} \right].$$

Herein, μ^* is the Coulomb pseudopotential and used to describe the interaction between electrons (μ^* = 0.1). In addition, the EPC constant, λ, and the logarithmic average phonon frequency, ω_{log}, are calculated with the Eliashberg spectral function for electron-phonon interaction:

$$\alpha^2F(\omega) = \frac{1}{N(E_F)} \sum_{kq,v} |g_{k,k+q,v}|^2 \delta(\varepsilon_k) \delta(\varepsilon_{k+q}) \delta(\omega - \omega_{q,v})$$

where $\lambda = 2\int d\omega \frac{\alpha^2F(\omega)}{\omega}$; $\omega_{log} = exp\left[\frac{2}{\lambda}\int \frac{d\omega}{\omega} \alpha^2F(\omega) ln(\omega)\right]$. Here, $N(E_F)$ is the electronic DOS at the E_F, $\omega_{q,v}$ is the phonon frequency of mode v and wave vector q, and $|g_{k,\,k+q,\,v}|$ is the electron-phonon matrix element between two electronic states with momenta k and $k + q$ at the E_F.

The work function (Φ) of a metal is calculated by considering a surface slab with a thickness of at least ten atoms. The vacuum distance is set to 20 Å, and a slab supercell is made with a, b > 10 Å. The Φ value is determined considering the difference between the vacuum potential and the Fermi level of the slab.[15]

Supporting Figures

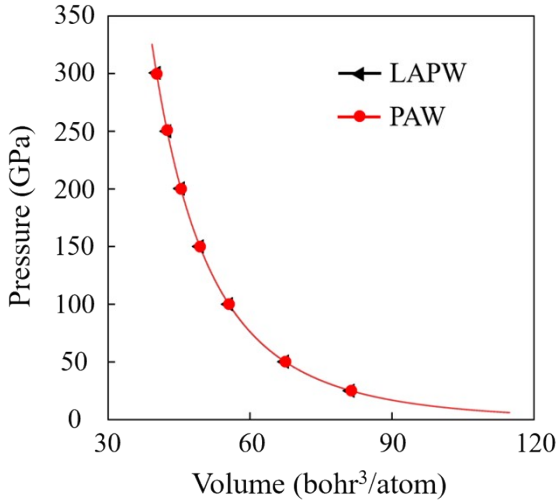

Figure S1. Comparison of the fitted Birch-Murnaghan equation of states for *Fm*-3*m* Li_3Sb by using the calculated results with the PAW pseudopotentials and full-potential LAPW methods.

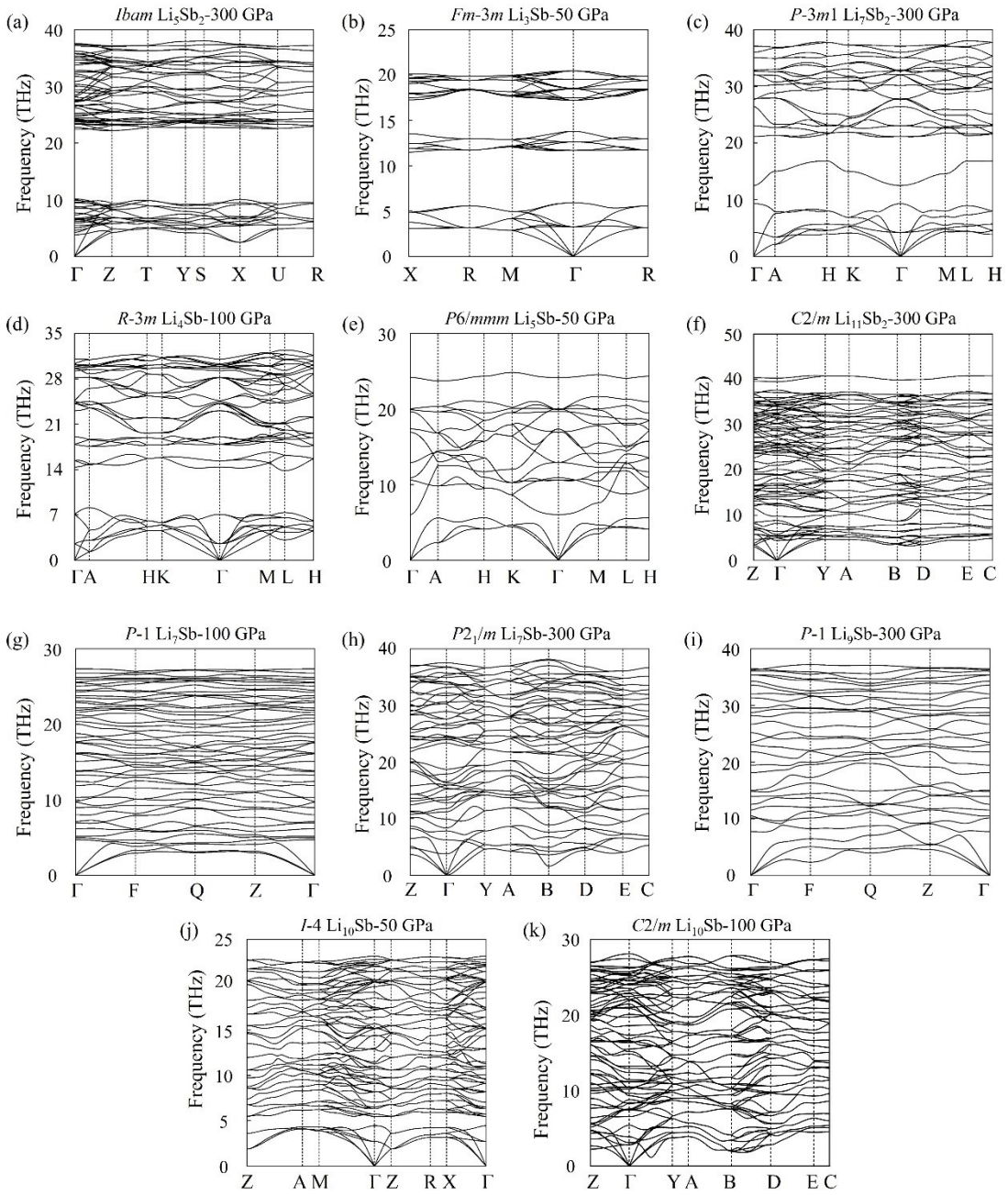

Figure S2. Phonon dispersion curves of Li-Sb compounds. (a) *Ibam* Li_5Sb_2 at 300 GPa, (b) *Fm*-3*m* Li_3Sb at 50 GPa, (c) *P*-3*m*1 Li_7Sb_2 at 300 GPa, (d) *R*-3*m* Li_4Sb at 100 GPa, (e) *P*6/*mmm* Li_5Sb at 50 GPa, (f) *C*2/*m* $Li_{11}Sb_2$ at 300 GPa, (g) *P*-1 Li_7Sb at 100 GPa, (h) $P2_1/m$ Li_7Sb at 300 GPa, (i) *P*-1 Li_9Sb at 300 GPa, (j) *I*-4 $Li_{10}Sb$ at 50 GPa, and (k) *C*2/*m* $Li_{10}Sb$ at 100 GPa. The calculated phonon dispersion curves show no imaginary modes in the whole Brillouin zone, indicating that all the predicted phases are dynamically stable.

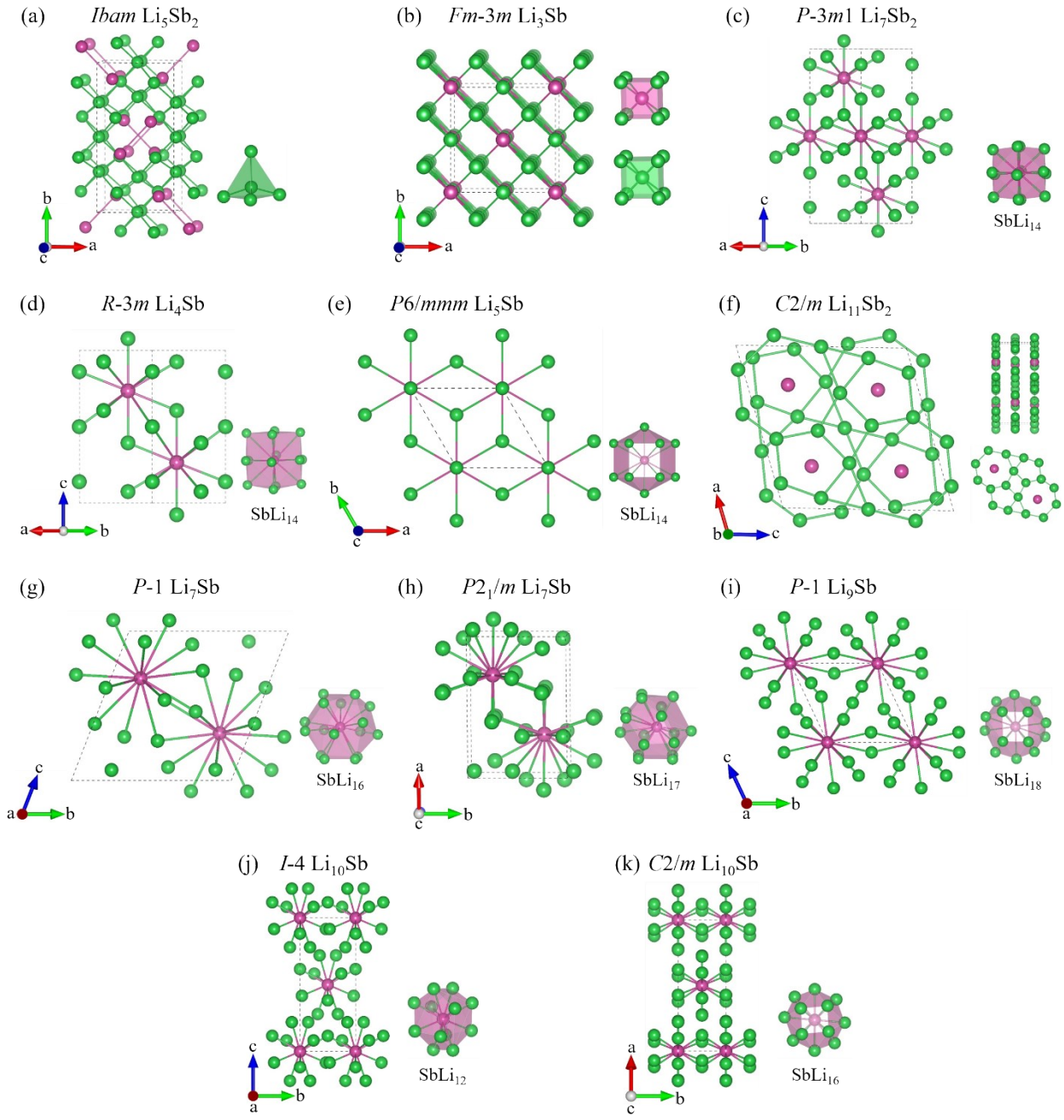

Figure S3. Crystal structures of (a) *Ibam* Li_5Sb_2, (b) *Fm*-3*m* Li_3Sb, (c) *P*-3*m*1 Li_7Sb_2, (d) *R*-3*m* Li_4Sb, (e) *P*6/*mmm* Li_5Sb, (f) *C*2/*m* $Li_{11}Sb_2$, (g) *P*-1 Li_7Sb, (h) $P2_1/m$ Li_7Sb, (i) *P*-1 Li_9Sb, (j) *I*-4 $Li_{10}Sb$, and (k) *C*2/*m* $Li_{10}Sb$.

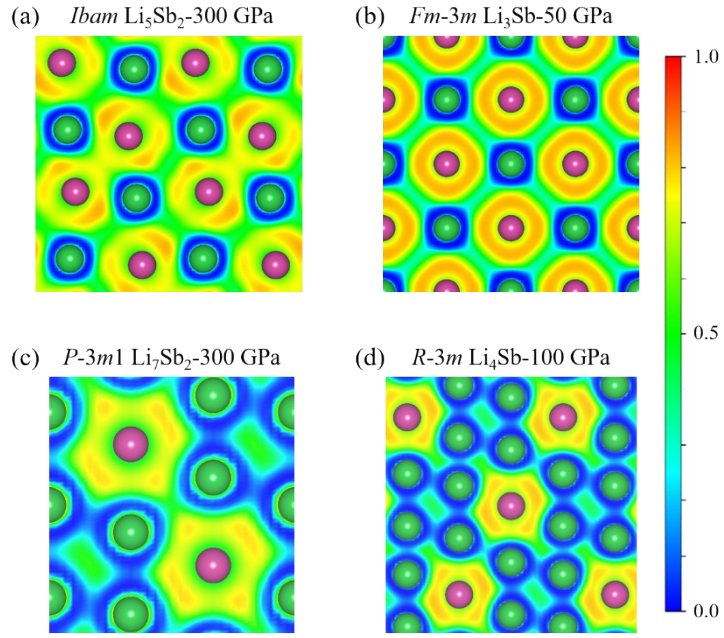

Figure S4. The ELF maps of (a) *Ibam* Li_5Sb_2, (b) *Fm*-3*m* Li_3Sb, (c) *P*-3*m*1 Li_7Sb_2, and (d) *R*-3*m* Li_4Sb. The absence of electron localization in their lattice interstitials indicates that they are not electrides.

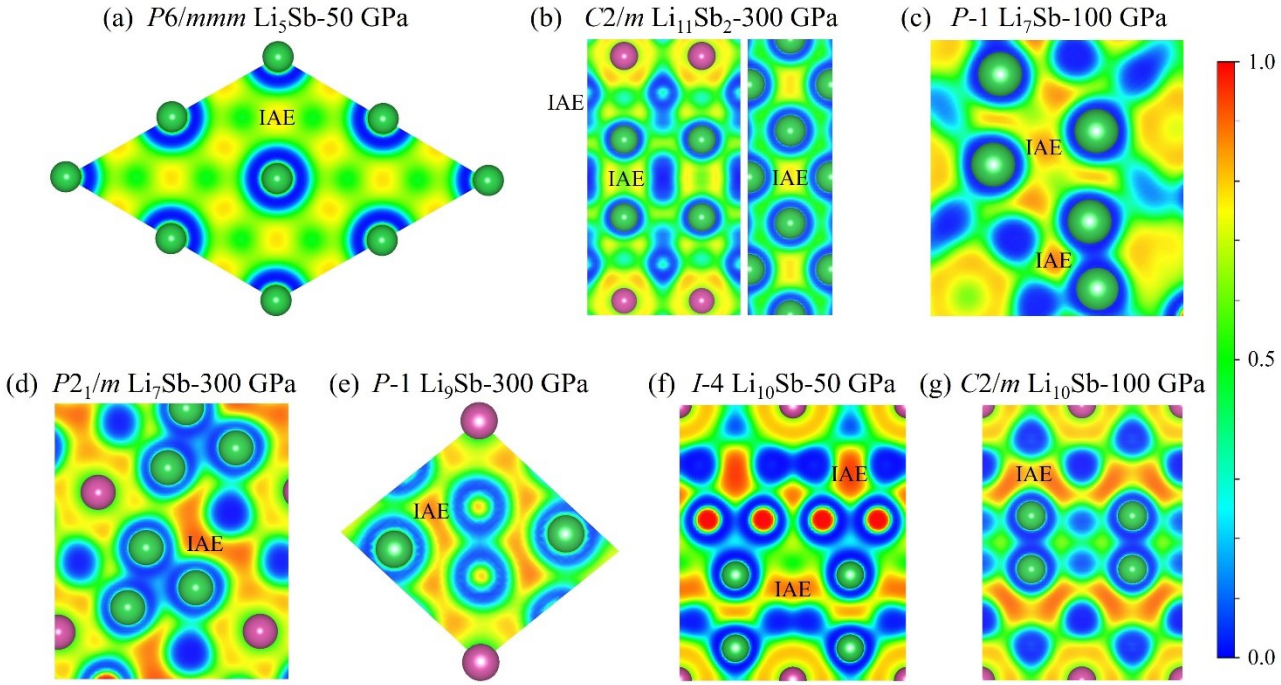

Figure S5. The ELF maps of (a) *P*6/*mmm* Li_5Sb, (b) *C*2/*m* $Li_{11}Sb_2$, (c) *P*-1 Li_7Sb, (d) $P2_1/m$ Li_7Sb, (e) *P*-1 Li_9Sb, (f) *I*-4 $Li_{10}Sb$, and (g) *C*2/*m* $Li_{10}Sb$. The presence of obvious electron localization in their lattice interstitials indicates that they are electrides.

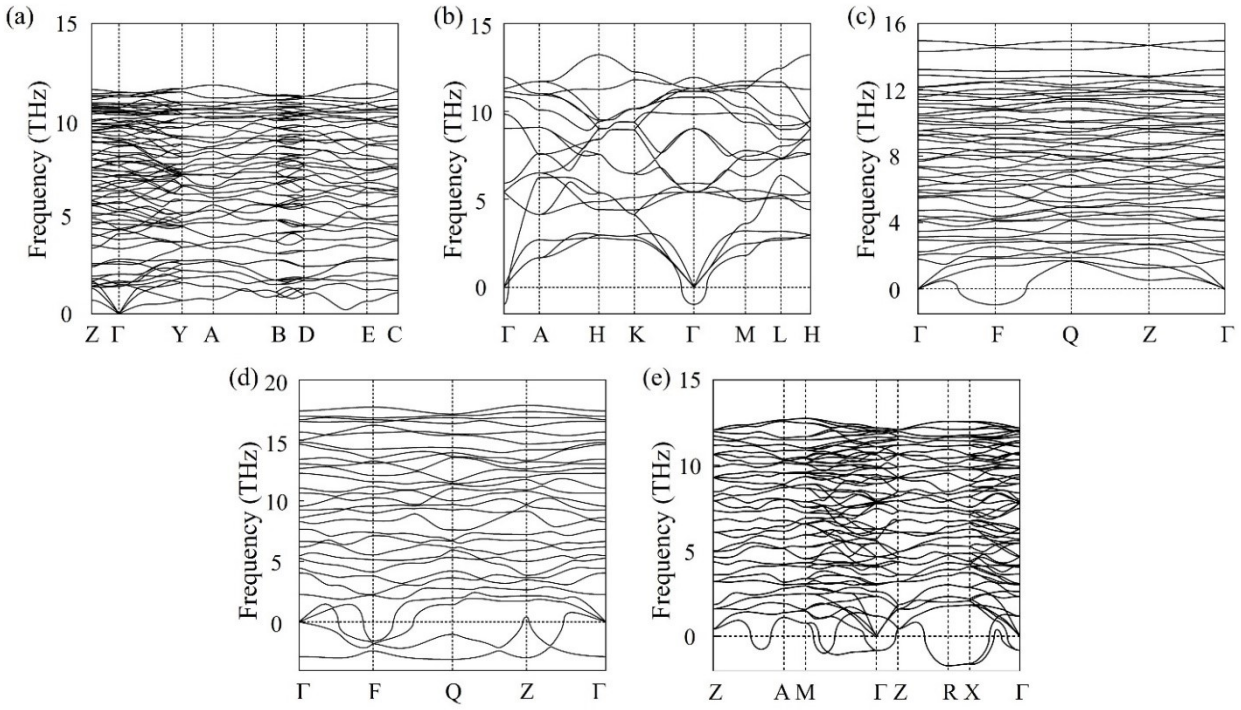

Figure S6. Phonon dispersion curves of (a) *C*2/*m* $Li_{11}Sb_2$, (b) *P*6/*mmm* Li_5Sb, (c) *P*-1 Li_7Sb, (d) *P*-1 Li_9Sb, and (e) *I*-4 $Li_{10}Sb$ at 0 GPa.

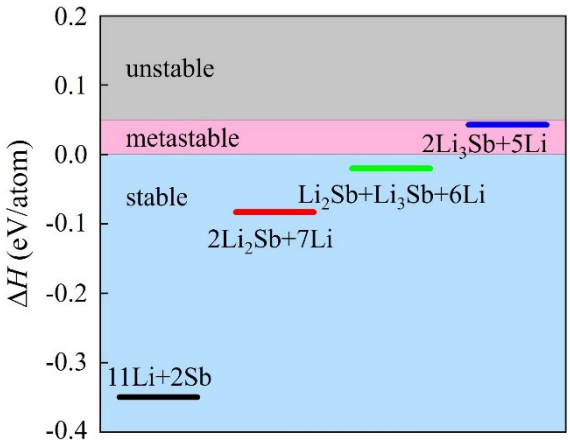

Figure S7. The formation enthalpies (Δ*H*) of *C*2/*m*-II $Li_{11}Sb_2$ along different synthetic paths at 0 GPa. The largest Δ*H* is 42.7 meV/atom with Li_3Sb and Li as reactants, suggesting that *C*2/*m*-II $Li_{11}Sb_2$ satisfies the criterion of metastable compound (<50 meV/atom).

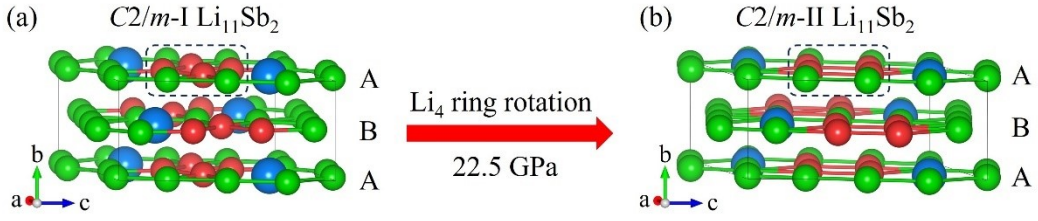

Figure S8. The side view of layered (a) *C*2/*m*-I and (b) *C*2/*m*-II. Li and Sb atoms are represented by green and blue spheres, respectively. The rotated Li_4 rings are highlighted with red.

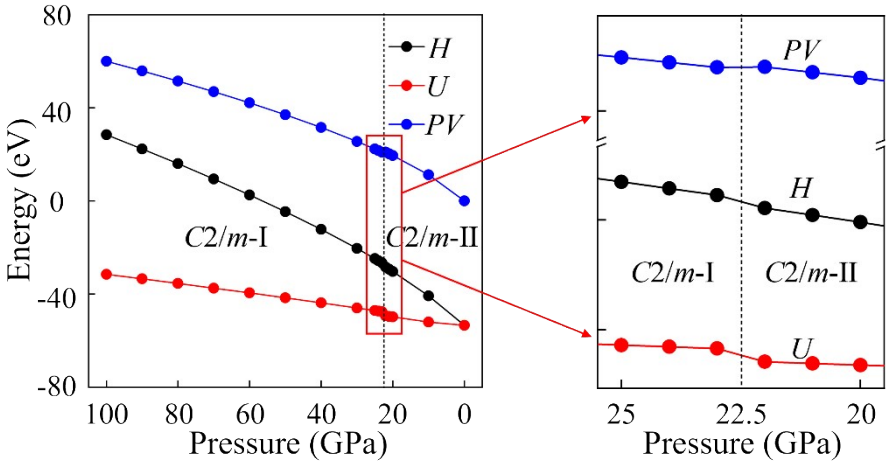

Figure S9. Enthalpy (*H*), internal energy (*U*), and the *PV* term as a function of pressure for these two phases of *C*2/*m* $Li_{11}Sb_2$. The right is the enlarged diagram of the red frame in the left.

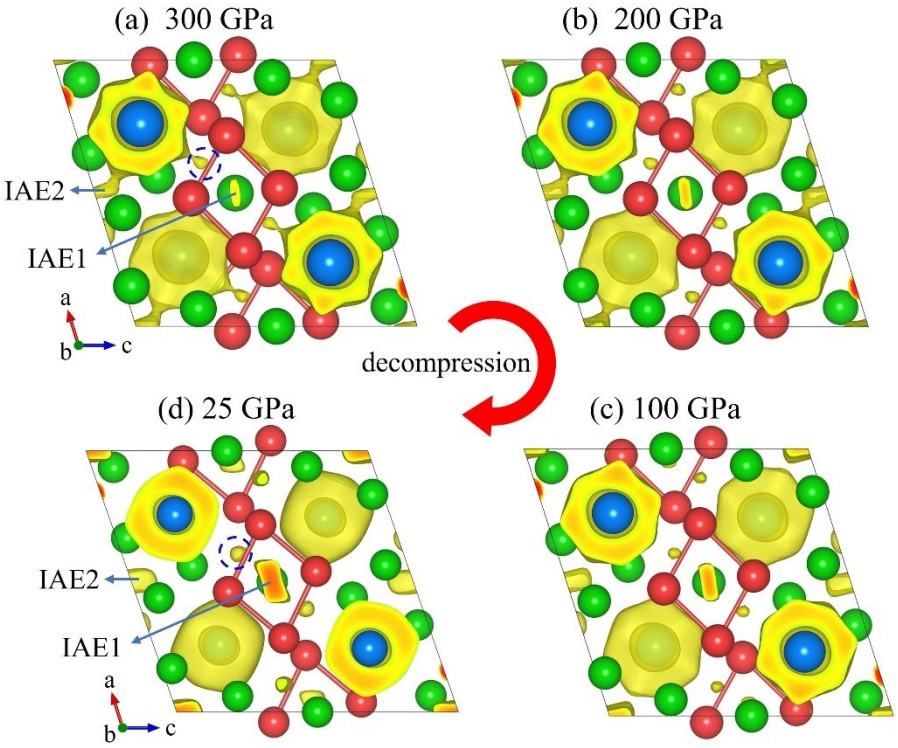

Figure S10. The change of IAEs during depressurization of *C*2/*m* $Li_{11}Sb_2$. With depressurizing, IAE1 and IAE2 gradually increase, IAE2 and Sb atom are separated from each other, and a small amount of electrons detach from Sb atoms (circled with dashed lines).

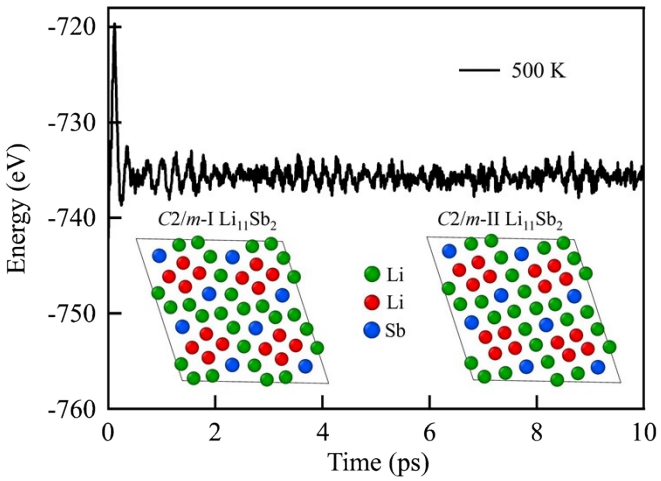

Figure S11. Total energy as a function of MD time for *C*2/*m*-I $Li_{11}Sb_2$ at 25 GPa and 500 K. The insets show the snapshots before (*C*2/*m*-I phase) and after (*C*2/*m*-II phase) a 10 ps AIMD simulation. The rotated Li_4 rings are highlighted with red.

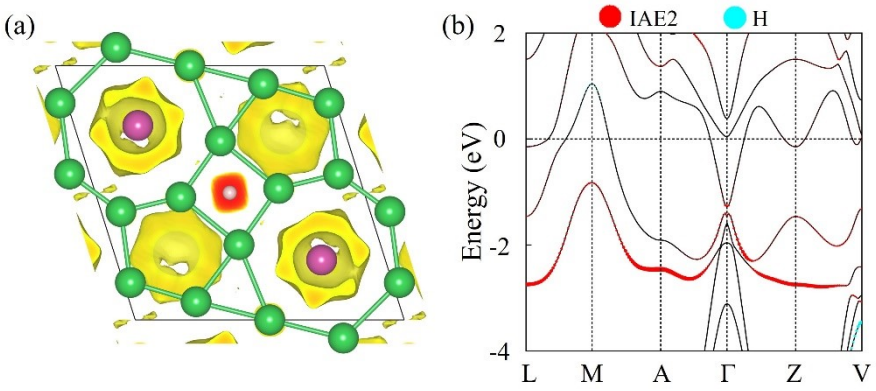

Figure S12. (a) The constructed hydrogenated model by inserting a hydrogen atom into the IAE1 site. (b) Projected electronic bands structure of hydrogenated model for *C*2/*m*-I $Li_{11}Sb_2$. It is noted that the isolated IAE1 hardly contributes to the band crossing the E_F after inserting a hydrogen atom into the IAE1 site.

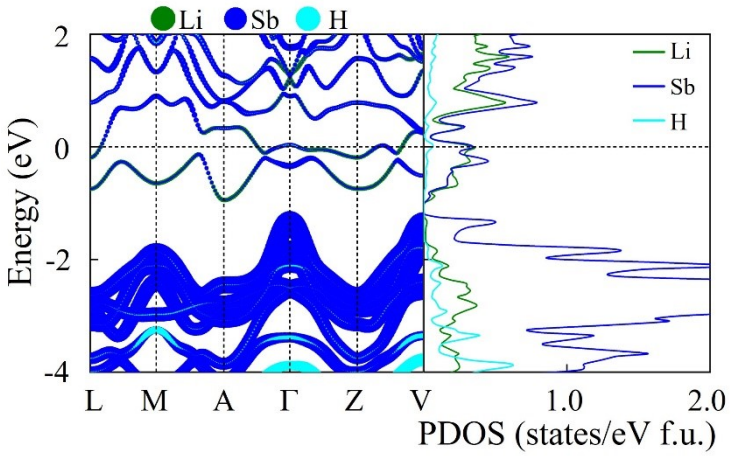

Figure S13. Projected electronic bands and density of states (DOS) of hydrogenated model for *C*2/*m*-II $Li_{11}Sb_2$.

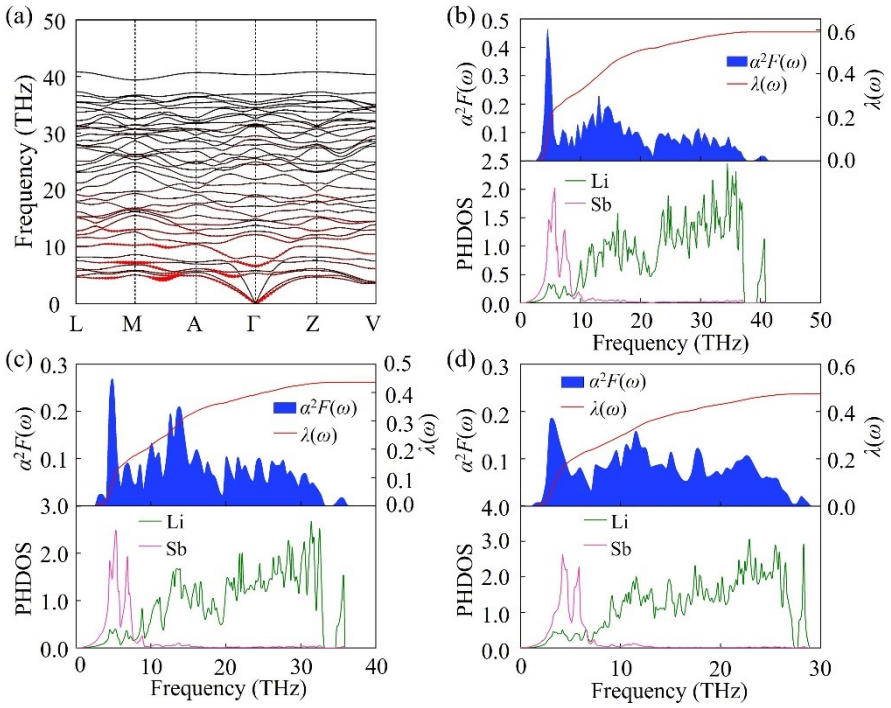

Figure S14. (a) The phonon dispersion curves with λ weights of $C2/m$-I $Li_{11}Sb_2$ at 300 GPa. PHDOS, Eliashberg spectral function $\alpha^2F(\omega)$, and frequency-dependent EPC parameters $\lambda(\omega)$ of $C2/m$-I $Li_{11}Sb_2$ at (b) 300 GPa, (c) 200 GPa, (d) 100 GPa.

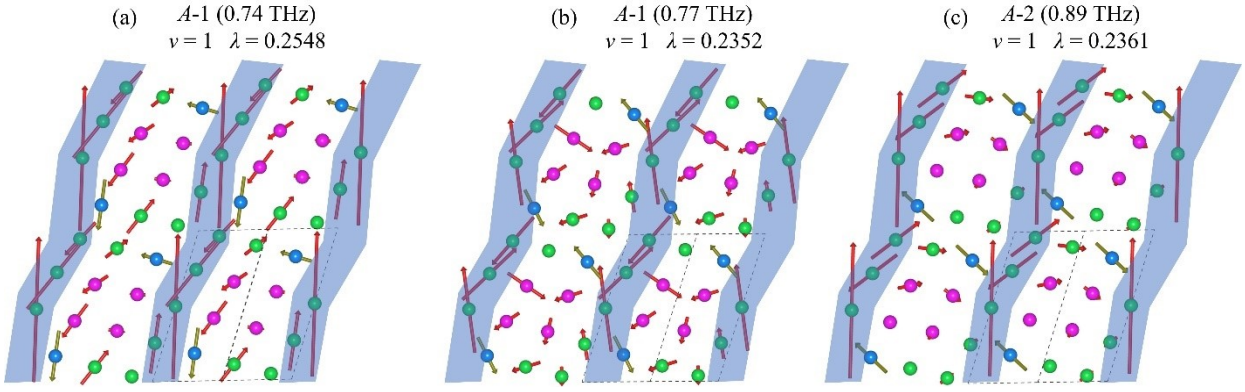

Figure S15. The three vibrational modes with the largest contribution to total λ in $C2/m$-II $Li_{11}Sb_2$ marked in the main text. A-1 modes at (a) 0.74 THz and (b) 0.77 THz, (c) A-2 mode at 0.89 THz. The largest vibrational vectors, associated with the Li atoms around the Li_4 rings highlighted with red, are approximately parallel to the Li-Sb sublayer along a unique zigzag-like channel (represented by shadows).

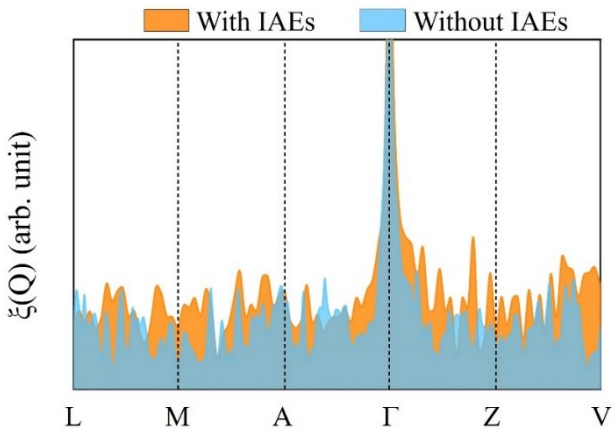

Figure S16. The Fermi surface nesting function ξ (Q) of $C2/m$-II $Li_{11}Sb_2$ with IAEs and without IAEs at 0 GPa.

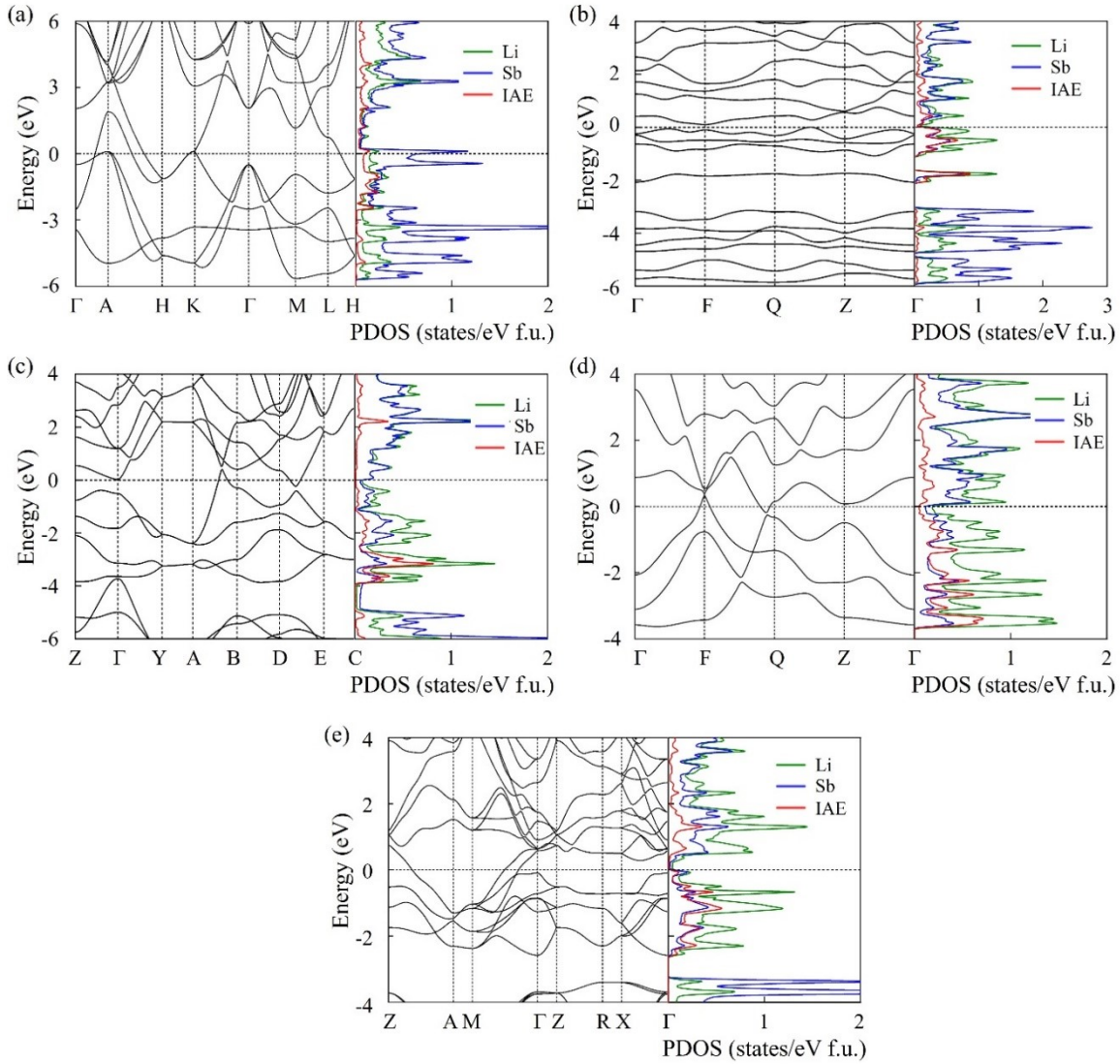

Figure S17. The electronic band structures and density of states (DOS) of electrides. (a) $P6/mmm$ Li_5Sb at 50 GPa, (b) P-1 Li_7Sb at 100 GPa, (c) $P2_1/m$ Li_7Sb at 300 GPa, (d) P-1 Li_9Sb at 300 GPa, and (e) I-4 $Li_{10}Sb$ at 50 GPa.

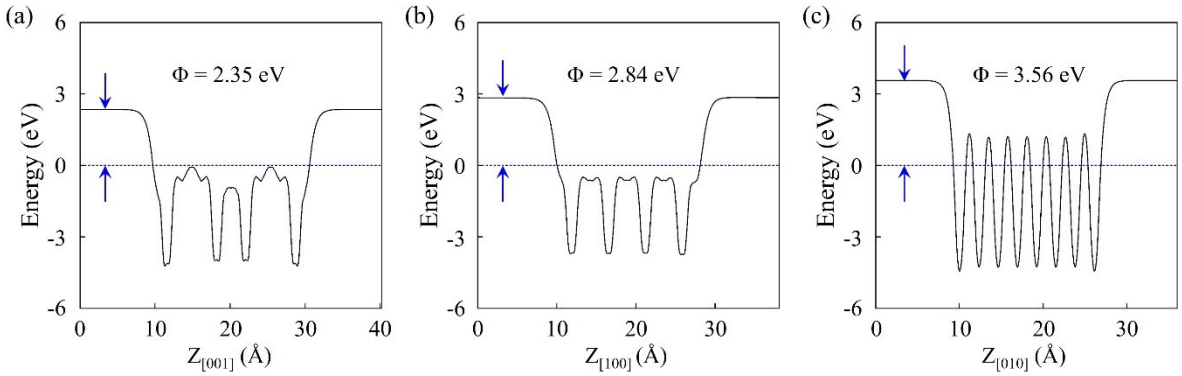

Figure S18. The work function of *C*2/*m*-II $Li_{11}Sb_2$ in (a) (001), (b) (100), and (c) (010) planes at 0 GPa. The Fermi level is set to zero.

Supporting Tables

Table S1. Bader charge analysis of Li-Sb electrides. The negative and positive values represent losing and gaining electrons in per formula unit, respectively.

Phase	Pressure (GPa)	Li	Sb	IAEs
*P*6/*mmm* Li_5Sb	50	-3.68 e^-	2.73 e^-	0.95 e^-
*C*2/*m* $Li_{11}Sb_2$	300	-6.44 e^-	5.62 e^-	0.82 e^-
P-1 Li_7Sb	100	-4.79 e^-	2.99 e^-	1.80 e^-
P2_1/*m* Li_7Sb	300	-4.20 e^-	2.83 e^-	1.38 e^-
P-1 Li_9Sb	300	-5.38 e^-	3.76 e^-	1.62 e^-
I-4 $Li_{10}Sb$	50	-7.07 e^-	3.11 e^-	3.96 e^-
*C*2/*m* $Li_{10}Sb$	100	-6.80 e^-	3.28 e^-	3.52 e^-

Table S2. The superconducting parameters and the contributions of different-frequencies phonons to λ of $Li_{11}Sb_2$ at different pressures. LF and MHF represent Sb-dominated low frequency vibrations and Li-dominated medium-high frequency vibrations (unit: THz), respectively.

Pressure (GPa)	T_c (K)	ω_{log} (K)	λ	LF (Sb)	λ(Sb%)	MHF (Li)	λ(Li%)
300	9.4	429.37	0.59	0-8.7	50.8%	8.7-41.7	49.2%
200	3.1	466.38	0.44	0-7.8	40.5%	7.8-36.6	59.5%
100	3.4	338.80	0.47	0-6.6	48.8%	6.6-29.0	51.2%
0	1.5	117.64	0.50	0-3.1	55.0%	3.1-13.1	45.0%

Table S3. The superconducting parameters of metallic Li-Sb electrides.

Phase	Pressure (GPa)	T_c (K)	ω_{log} (K)	λ
*P*6/*mmm* Li_5Sb	50	0.0	452.14	0.15
$P2_1/m$ Li_7Sb	300	1.0	604.15	0.35
P-1 Li_9Sb	300	0.0	560.65	0.19
I-4 $Li_{10}Sb$	50	1.7	328.01	0.42
*C*2/*m* $Li_{10}Sb$	100	9.2	189.22	0.81

Table S4. Structural information of stable Li-Sb compounds.

Phase	Pressure (GPa)	Lattice Parameters (Å)	Wyckoff Positions (fractional)			
			Atoms	*x*	*y*	*z*
Ibam Li_5Sb_2	300	$a = 4.5089$	Li (8g)	-0.00000	0.26851	0.25000
		$b = 8.7301$	Li (8j)	0.25891	0.86765	0.50000
		$c = 4.3295$	Li (4b)	0.50000	-0.00000	0.25000
		$\alpha = \beta = \gamma = 90°$	Sb (8j)	0.80064	0.10796	-0.00000
Fm-3*m* Li_3Sb	50	$a = 5.4678$	Li (8c)	0.25000	0.75000	0.75000
		$b = 5.4678$	Li (4a)	0.00000	0.00000	0.00000
		$c = 5.4678$	Sb (4b)	0.50000	0.00000	0.00000
		$\alpha = \beta = \gamma = 90°$				
P-3*m*1 Li_7Sb_2	300	$a = 3.1800$	Li (2c)	0.00000	0.00000	0.85965
		$b = 3.1800$	Li (2d)	0.33333	0.66667	0.60578
		$c = 5.7561$	Li (2d)	0.33333	0.66667	0.92435
		$\alpha = \beta = 90°$	Li (1b)	0.00000	0.00000	0.50000
		$\gamma = 120°$	Sb (2d)	0.66667	0.33333	0.73452

R-3*m* Li_4Sb	100	$a = 3.5893$ $b = 3.5893$ $c = 10.6211$ $\alpha = \beta = 90°$ $\gamma = 120°$	Li (6c) Li (6c) Sb (3b)	0.00000 0.00000 0.00000	0.00000 -0.00000 -0.00000	0.09090 0.28792 0.50000
*P*6/*mmm* Li_5Sb	50	$a = 3.7628$ $b = 3.7628$ $c = 4.6632$ $\alpha = \beta = 90°$ $\gamma = 120°$	Li (4h) Li (1a) Sb (1b)	0.33333 0.00000 0.00000	0.66667 0.00000 0.00000	0.24592 0.00000 0.50000
*C*2/*m* $Li_{11}Sb_2$	300	$a = 6.6555$ $b = 3.0885$ $c = 6.7011$ $\alpha = \gamma = 90°$ $\beta = 107.1945°$	Li (4i) Li (4i) Li (4i) Li (4i) Li (4i) Li (2c) Sb (4i)	0.21602 0.07419 0.98095 0.15124 0.06568 -0.00000 0.23897	0.50000 0.50000 0.50000 -0.00000 -0.00000 0.00000 -0.00000	0.53246 0.92159 0.33718 0.02863 0.24110 0.50000 0.76067
P-1 Li_7Sb	100	$a = 4.0345$ $b = 5.6070$ $c = 5.6587$ $\alpha = 67.7269°$ $\beta = 100.9708°$ $\gamma = 98.8763°$	Li (2i) Li (2i) Li (2i) Li (2i) Li (2i) Li (2i) Li (2i) Sb (2i)	0.90333 0.20709 0.36878 0.99966 0.57108 0.34229 0.29176 0.21843	0.44328 0.99024 0.57263 0.22588 0.77416 0.12494 0.38883 0.81348	0.26569 0.62022 0.08990 0.07084 0.70745 0.92753 0.53917 0.31646
*P*2$_1$/*m* Li_7Sb	300	$a = 5.4966$ $b = 3.6466$ $c = 3.9591$ $\alpha = \gamma = 90°$	Li (4f) Li (4f) Li (2e) Li (2e)	0.71110 0.95823 0.39983 0.40575	0.04274 0.94242 0.25000 0.25000	0.84838 0.79890 0.95166 0.52355

		β = 106.2418°	Li (2e)	0.09663	0.25000	0.66303
			Sb (2e)	0.71577	0.25000	0.34925
P-1 Li_9Sb	300	a = 3.3455	Li (2i)	0.50145	0.86559	0.24813
		b = 3.9021	Li (2i)	0.86109	0.82366	0.42030
		c = 3.9068	Li (2i)	0.44805	0.69400	0.70940
		α = 114.7651°	Li (2i)	0.77290	0.44916	0.87310
		β = 94.9633°	Li (1g)	0.00000	0.50000	0.50000
		γ = 93.2688°	Sb (1a)	0.00000	0.00000	0.00000
I-4 $Li_{10}Sb$	50	a = 4.3190	Li (8g)	0.24282	0.53371	0.91692
		b = 4.3190	Li (8g)	0.31849	0.64718	0.71970
		c = 10.3808	Li (4f)	0.00000	0.50000	0.11728
		$\alpha = \beta = \gamma$ = 90°	Sb (2a)	0.00000	0.00000	0.00000
*C*2/*m* $Li_{10}Sb$	100	a = 10.5025 b = 3.6232 c = 4.2427 $\alpha = \gamma$ = 90° β = 70.9186°	Li (4i)	0.22190	-0.00000	0.61368
			Li (4i)	0.90346	-0.00000	0.58217
			Li (4i)	0.77259	-0.00000	0.99942
			Li (4i)	0.07246	0.50000	0.24763
			Li (4i)	0.12089	0.50000	0.73105
			Sb (2a)	0.00000	0.00000	0.00000

References

1. Y. Wang, J. Lv, L. Zhu and Y. Ma, *Phys. Rev. B*, 2010, **82**, 094116.
2. Y. Wang, J. Lv, L. Zhu and Y. Ma, *Comput. Phys. Commun.*, 2012, **183**, 2063-2070.
3. G. Kresse and J. Furthmüller, *Phys. Rev. B*, 1996, **54**, 11169-11186.
4. P. Hohenberg and W. Kohn, *Phys. Rev.*, 1964, **136**, B864-B871.
5. W. Kohn and L. J. Sham, *Phys. Rev.*, 1965, **140**, A1133-A1138.
6. J. P. Perdew, J. A. Chevary, S. H. Vosko, K. A. Jackson, M. R. Pederson, D. J. Singh and C. Fiolhais, *Phys. Rev. B*, 1992, **46**, 6671-6687.
7. H. J. Monkhorst and J. D. Pack, *Phys. Rev. B*, 1976, **13**, 5188-5192.
8. P. E. Blöchl, *Phys. Rev. B*, 1994, **50**, 17953-17979.
9. A. Togo, F. Oba and I. Tanaka, *Phys. Rev. B*, 2008, **78**, 134106.
10. P. Blaha, K. Schwarz, P. Sorantin and S. B. Trickey, *Comput. Phys. Commun.*, 1990, **59**, 399-415.
11. G. Kresse and J. Hafner, *Phys. Rev. B*, 1993, **47**, 558-561.
12. P. Giannozzi, S. Baroni, N. Bonini, M. Calandra, R. Car, C. Cavazzoni, D. Ceresoli, G. L.

Chiarotti, M. Cococcioni, I. Dabo, A. Dal Corso, S. de Gironcoli, S. Fabris, G. Fratesi, R. Gebauer, U. Gerstmann, C. Gougoussis, A. Kokalj, M. Lazzeri, L. Martin-Samos, N. Marzari, F. Mauri, R. Mazzarello, S. Paolini, A. Pasquarello, L. Paulatto, C. Sbraccia, S. Scandolo, G. Sclauzero, A. P. Seitsonen, A. Smogunov, P. Umari and R. M. Wentzcovitch, *J. Phys. Condens. Matter*, 2009, **21**, 395502.

13. P. B. Allen and R. C. Dynes, *Phys. Rev. B*, 1975, **12**, 905-922.
14. R. C. Dynes, *Solid State Commun.*, 1972, **10**, 615-618.
15. M. A. Uijttewaal, G. A. d. Wijs and R. A. d. Groot, *J. Appl. Phys.*, 2004, **96**, 1751-1753.